Eur. Phys. J. B (2021)94:96
https://doi.org/10.1140/epjb/s10051-021-00106-x

THE EUROPEAN PHYSICAL JOURNAL B

Regular Article - Solid State and Materials

Improvement electronic and magnetic properties of Cr impurity doped PbSe for optoelectronic devices applications: a first-principles proposal

Amel Benkada[1,4], Salem Habri[2], Bouzouira Nour Eddine[3], Djillali Bensaid[1,4,a], Meryem Hamli[1], and Bencherif Kaddour[1]

[1] Faculty of Science and Technology, University Belhadj Bouchaib, BP 284, 46000 Ain-Temouchent, Algeria
[2] Ecole Normale Supérieure d'Oran, BP 1063 Saim Mohamed, 31003 Oran, Algeria
[3] University Centre Nour Bachir El Bayadh, El Bayadh, Algeria
[4] Laboratory Physico-Chemistry of Advanced Materials, University of Djillali Liabes, Sidi-Bel-Abbes 22000, Algeria

Received 18 February 2021 / Accepted 19 April 2021
© The Author(s), under exclusive licence to EDP Sciences, SIF and Springer-Verlag GmbH Germany, part of Springer Nature 2021

Abstract. To produce innovative spintronics components, we are now looking for ferromagnetic semiconductors at room temperature. The aim of this work is to study the electronic structures and the magnetic properties is to trigger ferromagnetism and to improve the band gap of PbSe The study of the electronic structure and the magnetic properties of diluted magnetic semiconductors (DMS) type IV–VI PbSe doped Cr is investigated in detail. Our results are as follows. We then calculated the sp-d exchange couplings between electrons (holes) of the conduction (valence) band and magnetic impurities. The topology of the band structure shows that our material is half metal, which has a direct gap in the minority channel due to the nature of sp–d coupling. The values of Nα ferromagnetic and Nβ antiferromagnetic obtained in the mean-field approximation are of the order of 0.551 and −0.445 eV respectively. The Thermoelectric Conversion Efficiency focuses on a single dimension parameter, the figure of merit ZT. We have seen that doping with Cr can also have a beneficial effect on thermal conductivity and consequently on ZT. This leads our material among the best compounds to thermoelectric applications.

1 Introduction

Doped impurities in semiconductors provoke significant modification in their electronic, magnetic and optical properties, necessitating their industrial applications. Magnetic semiconductors involve doping magnetic elements in traditional semiconductors. Particularly, they can be used in the field of spintronics. In this context, the combination of charge and spin at the same time in new devices opened up a loophole in logic and information storage capacities.

The lead-based IV–VI semiconductor family possesses special electronic characteristics due to the interaction of the strongly occupied cation band with the p-valence electrons of the anion, elicited to sweep a large a number of different properties that can be used in different fields of application such as optics, superconductivity, or even magnetism. Due to their semiconductor property, these compounds have proven to be essential in thermoelectricity. The introduction of a magnetic element such as chromium in the host semiconductor leads the material to new characteristics. Type II–VI diluted magnetic semiconductors form an important class of DMS in which electrical doping and magnetic doping can be controlled independently. Lead-based chalcogenides doped with a magnetic ion are a new class of DMS that is still poorly understood and the nature of the magnetic interactions remains to be elucidated. The p-type doping of type IV–VI DMS is a challenge and the control of magnetic interactions by electrical doping could result in a ferromagnetic DMS at room temperature [1–4]. Cr-doped n-type PbSe with small carrier concentration is a thermoelectric (TE) material which attracts increased attention for larger average merit figures ZT value wide temperature range (300–873 K) [5], another similar material as Cr rich PbSe has long range FM coupling order and becomes half metallic, this is Cr doped PbS [6]. Transition metal-doped IV–VI semiconductors, accuracy Ge–Sb–Te-based materials (TM-GST) have gained attention for their high performance and reliability. in the work of Wang et al. [7], where they combine the experimental and the DFT proved that doping with chromium leads to a Ge1Sb2Te4 type structure. these results provide a novel approach for the fabrication of chalcogenide superlattices which are the best candidates for the next generation of nonvolatile data storage [7].

[a] e-mail: djizer@yahoo.fr (corresponding author)

Published online: 03 May 2021

2 Computational method

In the DFT framework, we have performed calculations using the FP-LAPW method implemented in the WIEN2k [8]. the stability structural, half-metallic ferromagnetic and magnetic properties are treated by the exchange-correlation potential the generalized gradient approximation (GGA) was used in the form proposed by Perdew et al. [9]. In this computation, a unit cell was divided into two regions where the plane waves is used in the interstitial region and spherical harmonic expansion was used for atomic spheres. The muffin tin sphere radiuses (RMT) are chosen in such ways to ensure that the charge will leak the atomic sphere. The muffin-tin sphere radii RMT were taken to be 2.5, 1.7 and 2.1 atomic units (au) for Pb, Cr and Se, respectively. RMT $\times K_{\max} = 9$ was used for the number of plane waves, and the expansion of the wave functions was set to $l_{\max} = 10$ inside of the muffin tin spheres, while the charge density was Fourier expanded up to $G_{\max} = 12$ a.u.$^{-1}$, where $G_{\max}$ is the largest vector in the Fourier expansion. A $12 \times 12 \times 12$ point mesh was used as base for the integration in The Brillouin zone sampling. The energy convergence criterion was set to 10^{-7} Ry

3 Results and discussion

3.1 Structural properties and stability of the Cr-doped PbSe

The binary IV–VI semiconductor PbSe crystallizes in the NaCI(B1) structure with a space group of 225(Fm3m), where the Pb atom occupies the top of the cube and the atom Se located at the center of the cube. For the $Pb_{1-x}Cr_xSe$ compounds, we used a super cell of 16 atoms and substituting one and too Pb cation sites by the Cr atoms to obtain the following fractions $Pb_{1-x}Cr_xSe$ ($x = 0.125$ and 0.25). For example in Fig. 1. We present the structure which corresponds to $x = 0.125$ and $x = 0.25$. To have the thermodynamic stability of the solid-state phase of doped systems, we calculate the formation energy by the following relation [10]:

$$E_F = E\,(\text{doped}) - E\,(\text{pure}) + \mu_{Pb} - \mu_{Cr}$$

Where the terms E (doped), E (pure), μ_{Pb} and μ_{Cr} are the total energy of the doped PbSe, the total energy of the pure PbSe, the chemical potentials for Pb and Cr atoms, respectively. By using this definition the formation energy is negative for all fractions Cr confirms that the Cr-doped PbSe exhibits a good structural stability The calculated negative formation energies are −17.7 and −17 eV of $Pb_{1-x}Cr_xSe$ ($x = 0.125$ and 0.25) compounds illustrate that the compounds formation in the FM state is more favorable (see Table 1). The curve analysis $E(V)$ (E = total energies, V = cell volumes) with adjustment by the empirical Murnaghan equation of state [11] leads to determine the equilibrium lattice constant (a), the volume modulus (B) and its pressure derivative (B'). Figure 2 Show the linearity of decrease the lattice constant with increase fraction doped-Cr The decrease of the lattice parameters with Mn concentration may be attributed to the large ionic radius of Cr^{3+} (1.66 Å) compared to that Se^{2+} (1.03 Å). This decrease in lattice parameter can be further explained by a start of the formation of the secondary phase and a decrease in the default concentration. The replacement of Cr by Pb influences the bond length which causes a small crystal distortion in the crystal structure, The calculated lattice parameter a (Å) versus concentration was fitted by a polynomial order 3 equation gives a very small deviation:

$$a\,(\mathring{A}) = 6.2711 - 0.925x - 0.066x^2 - 0.0042x^3$$

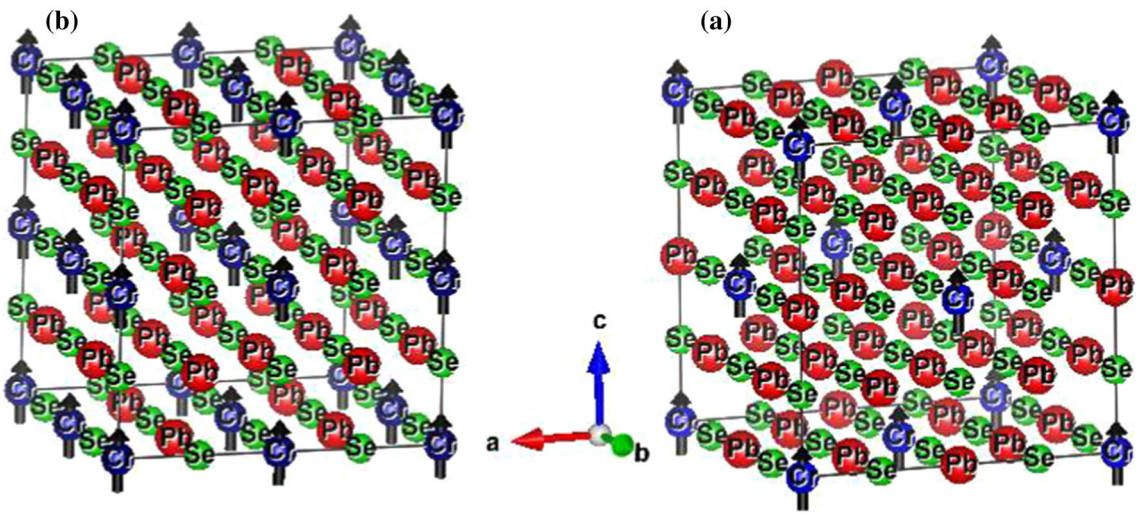

Fig. 1 The crystal structures of $Pb_{1-x}Cr_xSe$ compounds with : **a** $x = 0.125$, **b** $x = 0.25$ supercell of 16 atoms

Table 1 Calculated lattice constant (a), bulk modulus (B), half-metallic ferromagnetic band gap E_g and half-metallic gap for $Pb_{1-x}Cr_xSe$

$Pb_{1-x}Cr_xSe$	a (Å)	B (GPa)	B'	E_F (eV)	E_{HMF} (eV)	E_{HM} (eV)
$x = 0.125$	6.1416	49.47	3.77	−17.704	0.39	0.07
$x = 0.25$	6.051	51.69	3.38	−17	0.304	0.017

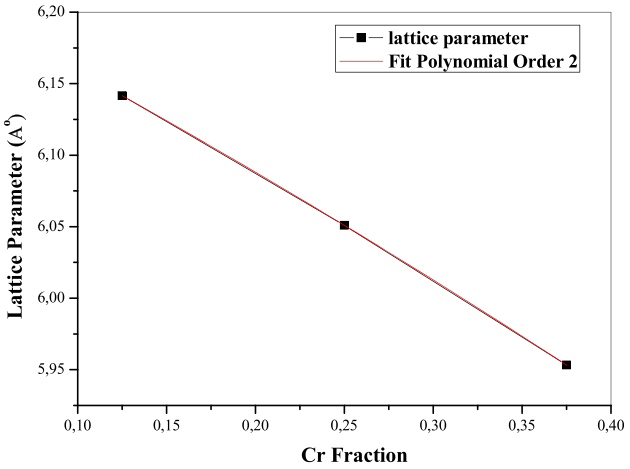

Fig. 2 Variation in lattice constants a of $Pb_{1-x}Cr_xSe$ as a function of composition x

3.2 Band structure and density of states property

The study of electronic properties consists of analyzing the band structure to know the effect of the magnetic impurity. The band structure is determined in the along the high symmetry directions in the Brillouin zone. The existence of a high symmetry between majority and minority spin and the position of EF in gap of minority channel proves that the system is a half-metallic character (see Fig. 3a). The $Pb_{0.875}Cr_{0.125}Se$ have an direct gap at Γ point. The half-metallic ferromagnetic band (HMF) gap E_g value obtained is 0.39 eV and half-metallic (HM) gap G_{hm} equal 0.07 eV this last one is very important in spintronic applications. The increases of Cr ions in the crystal lattice provoke the growth of electrons in the conduction band which leads to the insulator-metal transition [12,13]. the addition 0.125 of Cr quantity induce a decrease in the band gap (EHFM) by 0.09 eV and a slight increase in the half-metallic gap by a 0.01 eV (see Table 1), this overlap in the gap is due to the increase in spd exchange interaction between band electrons and localized 3d electrons of the transition metal atom [14,15].

We can see a gap in the majority spins if we move the fermi level towards the conduction band which leads the materials to a semiconductor character. this is a new class of materials called Spin-gapless semiconductors and according to Wang et al. [16] the practical use of SGS type II made by Fermi level tuning to achieve easy switching between electron and hole modes.

Chromium is the chemical species with the fewer electrons in the system, with the d orbital's unfilled. Therefore, this atom makes the main contribution to the occupied states of the minority spin states. The Fermi level is located in the band gap of the minority spin electrons, between the occupied d bands of the Cr atoms and of the states resulting from the hybridization of the d orbital's of the Cr and the p Pb. this hybridization provoke the double exchange interaction which is the principal cause of introducing ferromagnetism in the IV–VI doped Cr.

The chemical environment of the Cr atoms will be determining for the conservation of the half-metallicity. This information is consistent with that described in Fig. 3a, b, which show the contribution of Cr, Pb and Se atoms to energy bands, for majority and minority spin electrons

The spin up-flip energy (E^{sf+}) and the spin down-flip energy (E^{sf-}) measure an energy cost, whereas the down-flip is the spin counterpart to the ionization energy, while the up-flip is the spin counterpart to minus the electron affinity [17]. We calculated the difference of the spin-flip energies by the relationship: $E_s = E^{sf-} + E^{sf+}$

The chemical hardness in quantum chemistry is defined as the half between the deference of finite and ionization energy; similarly, we designate E_s as spin gaps stiffness. All this quantity is displayed in Table 3.

The calculations generally show the spin-flip gaps E^{sf+} (E^{sf-}) is 0.39 (0.215) and 0.398 (−0.077 eV) for $Pb_{0.75}Cr_0.25Se$, and $Pb_{0.75}Cr_{0.25}Se$ respectively (Table 2). These values indicated to intraband transitions across the pseudogap, and interband transitions across the spin gap. Since, the spin electronegativity χ is less than unity; we note that the down flip is energetically cheaper than to flip a spin up. Figure 4 shows the total and partial density of states for spin-up and spin down patterns for the $Pb_{1-x}Cr_xSe$ ($x = 0.125$ and 0.25) compounds.

the both edges of the band gap in the spin-down channel is principally composed of the hybridized 3d states of Cr and 6p states of Pb atoms, The DOS around EF are mainly participated by Cr-d states with small attribution of Se-p states which play the important role to provoke HM ferromagnetism in these compounds.

The reduced DOS near EF in spin-down channel is also seen in when substituting Cr in PbSe.

The Cr atom is surrounded by a tetrahedral environment, their d-orbital split into both orbitals t_{2g} and e_g. Owing to the substitution of the chromium, the entire electron in majority spin states Cr-d gets generated in

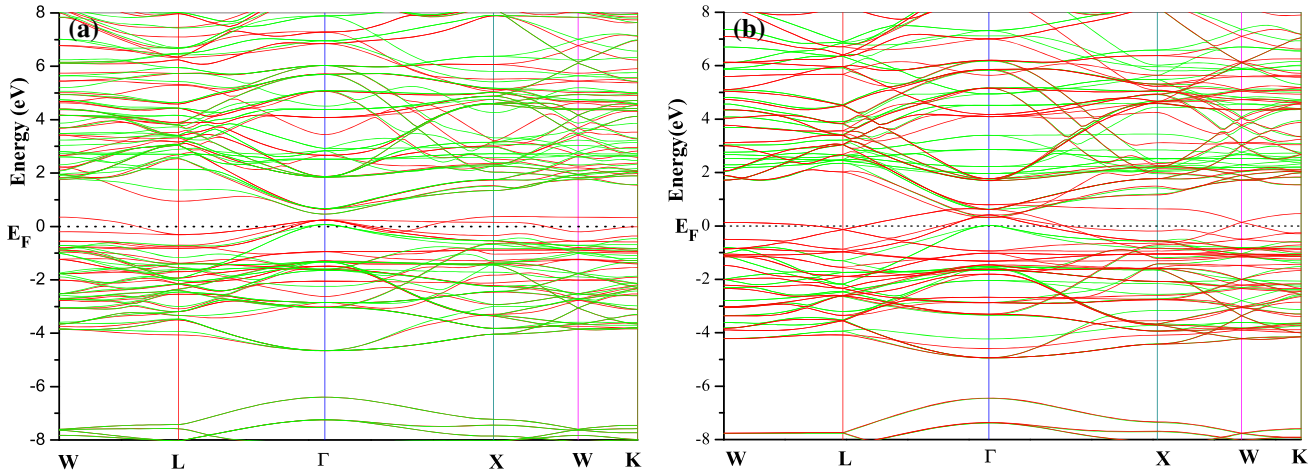

Fig. 3 Spin-polarized band structures for majority spin (up) (red line) and minority spin (dn) (green line) for $Pb_{1-x}Cr_xSe$. (**a** $x = 0.125$ and **b** 0.25)

Table 2 Calculated spin–flip gap E_s and the spin electronegativity χ for $Pb_{1-x}Cr_xSe$ ($x = 0.125$ and 0.25)

$Pb_{1-x}Cr_xSe$	$E^{sf+} = E_c^{\uparrow} - E_v^{\downarrow}$	$E^{sf-} = E_c^{\downarrow} - E_v^{\uparrow}$	E_s	$\chi^s = (E^{sf-} E^{sf+})/2$
$x = 0.125$	0.39	0.215	0.605	−0.0875
$x = 0.25$	0.398	−0.077	0.32	−0.237

Table 3 Calculated total and local magnetic moment (in μ_B) within the muffin-tin spheres and in the interstitial sites for $Pb_{1-x}Cr_xSe$

$Pb_{1-x}Cr_xSe$	M_{tot}	M_{Cr}	M_{Pb}	M_{Se}	M_{Inter}
$x = 0.125$	4.0148	3.129	0.0025	−0.042	1.047
$x = 0.25$	8.026	3.185	−0.0045	0.078	1.048

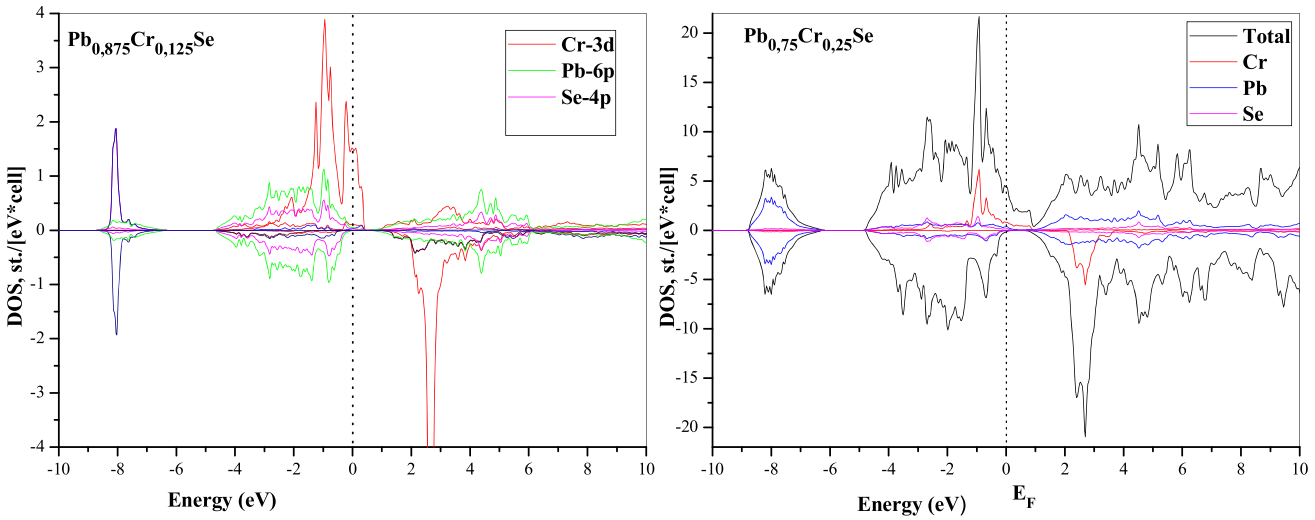

Fig. 4 Calculated spin polarized total and partial density of states for $Pb_{1-x}Cr_xSe$. ($x = 0.125$ and 0.25)

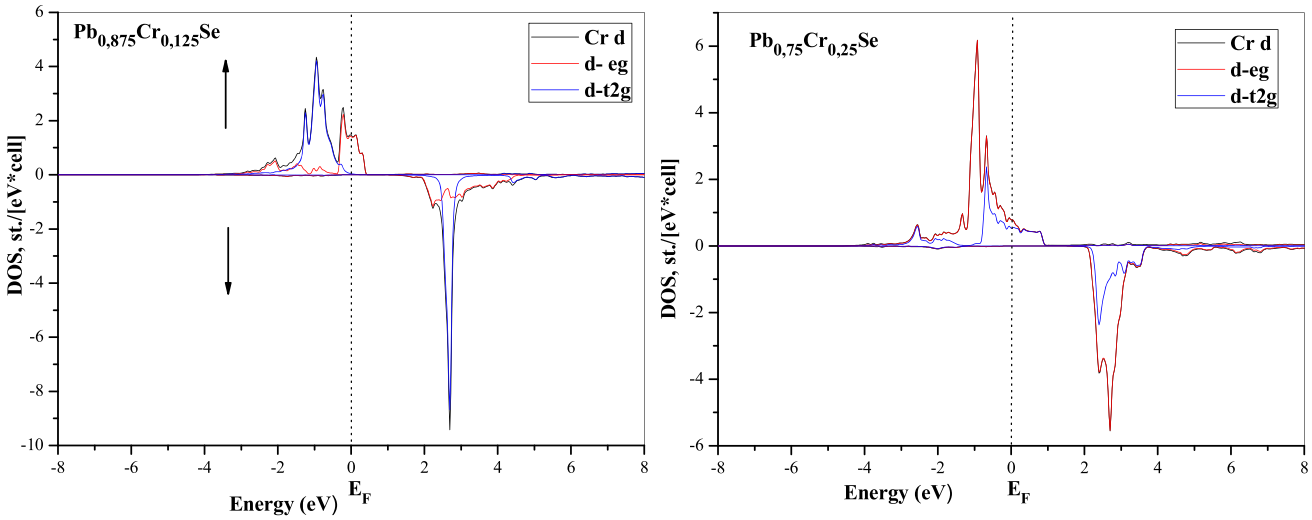

Fig. 5 Spin-resolved t_{2g} and e_g DOS of $Pb_{1-x}Cr_xSe$. ($x = 0.125$ and 0.25) in the FM configuration

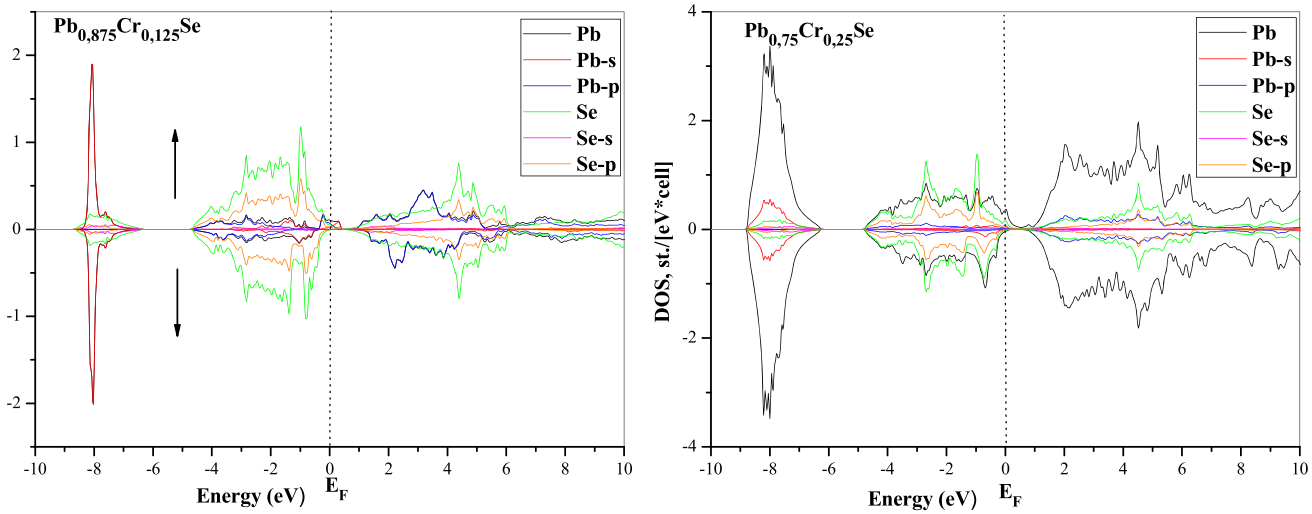

Fig. 6 Partial density of states (DOS) for Pb and Se atoms of $Pb1_{-x}Cr_xSe$. ($x = 0.125$ and 0.25) compound in the FM configuration

band gap. The five degenerate electrons of Cr atom in quantum states divide into t_2g and e_g states due the crystal field created by octahedral environment of Se atom. The effect of these two types of symmetric states is visualized in the TDOS (Fig. 5) for $Pb_{1-x}Cr_xSe$ at $x = 0.125$ and 0.25. the analysis of minoritory channel of the DOS, informed that the t_{2g} and e_g to contribute completely in CB for both the dopant concentrations and absent at EF but in majority channel the fraction for this state's crosses EF which indicate the metallic behavior.

We observe in Fig. 6, that the states s of Pb is probably does not play a role around Fermi energy because they are separated by other states by an energy gap of about 4 eV, Whereas the P–Se and P–Pb orbitals reside in conduction and valence bands around Fermi level, respectively.

When the impurity element Cr is incorporated into the matrix PbSe, it produces a significant change to the DOS of the matrix. The Cr 3d and Pb 6p states are located in the spin-up band gap, and the DOS spectral weight is relatively small but not negligible. the 6s states of Se are located in the low energy of the valence band on the other hand the 4p states are located near the fermi level in the valence band and almost symmetric for the two channels, this situation is noticed for both concentration. This behavior changes in the conduction band where we observe that the Pb 6p states have disappeared for the concentration 0.25 due to the increase magnetic impurities in the matrix which directly influences in the minority channel where the gap widens (see Fig. 6).

Table 4 Calculated conduction and valence band-edge spin splitting ΔE_c and ΔE_v and exchange constants $N_0\alpha$ and $N_0\beta$ for $Pb_{1-x}Cr_xSe$ ($x = 0.125$ and 0.25)

$Pb_{1-x}Cr_xSe$	$\Delta E_C = E_c^{\downarrow\cdot} - E_c^{\uparrow}$	$\Delta E_V = E_v^{\downarrow\cdot} - E_v^{\uparrow}$	$N_0\alpha$	$N_0\beta$
$x = 0.125$	0.21562	−0.17417	0.5513	−0.4453
$x = 0.25$	−0.076	−0.39827	−0.193	1.00

4 Magnetic properties and exchange coupling

Generally, the magnetism in Cr-based magnetic compounds is initially correlated with the crystal structure. i.e., lattice constant modifications strongly assign the magnetic interactions between the ions. according to the basis of the Heisenberg model which describes the various magnetic structures, we note that the coupling in our compounds is ferromagnetic because the type of the magnetic interaction is an exchange interaction between the Cr^{+3} ion with spin $3d^5$ and the a nearest neighbor. Indeed, the magnetism is due to the appearance of locale moment on Cr atoms. We have displayed in Table 3, the total magnetic moments for the two concentrations as well as the local magnetic moments of the Pb, Cr and Se atoms. We notice that the magnetic moment of Cr atom for the different concentrations remains around $\approx 3\mu_B$, which brings the total magnetic moment invariant. When introducing magnetic impurities into a cation site and due to crystal field, the 3d orbital's of the magnetic impurity split into the triply degenerate t_{2g} states and doubly degenerate e_g states. The magnetic moment of the atom Pb and Se is neglected which proves that the parents material is a semiconductor.

In magnetic compounds, The phenomenon where by individual atomic magnetic moments will attempt to align all other atomic magnetic moments within a material with itself is known as the exchange interaction [18], If the magnetic moments align in a parallel fashion, the material is ferromagnetic; if the magnetic moments align antiparallel, the material is antiferromagnetic.

The approximation of the mean field consists in replacing the spin operator in the Kondo Hamiltonian [19] by its mean value proportional to the magnetization. Reintroducing the translational invariance of the system and by neglecting the inter-band words.

With this approach, we can express the exchange constants $N_0\alpha$ and $N_0\beta$ as a function of the band edges spin splitting of the valence and conduction bands. These last constants are determined by the following relation [20,21]:

$$N_0 b\alpha = \frac{\Delta E_C}{x} \quad \text{and} \quad N_0\beta = \frac{\Delta E_V}{x}$$

With $\Delta E_C = E_c^{\downarrow\cdot} - E_c^{\uparrow}$ is the conduction band-edge spin splitting and $\Delta E_V = E_v^{\downarrow\cdot} - E_v^{\uparrow}$ is the valence band-edge spin splitting at the Γ symmetry point, x is the concentration of Cr, and $< s >$ is half of the computed magnetization per Cr ion

According to Table 4, the splitting of the valence band is antiferromagnetic because its value is negative; on the other hand the splitting of the conduction band is ferromagnetic (positive).

The peak appears on the diagrams of the density of state (Fig. 3) is characterized by a localized state or linked to the magnetic impurity of 3d character of Cr. the existence of two different splittings which mark the appearance of this localized stat. The splitting ΔE_V is a splitting between the spin down valence band and the localized spin up state which corresponds to the exchange $N_0\beta$ strongly antiferromagnetic (negative). Here we declare, that the effect of finite size translates by an increase in the width of the 3d bands of the transition metals caused by a greater overlap of the 3d states with the states of the valence band, which implies a decrease in the localization effect

5 Thermoelectric properties

The half-metallic compounds have been widely studied as promoter candidates in thermoelectricity for converting waste heat into electricity. Among this family of half-metallicity materials, heuslers and diluted magnetic semiconductors compounds which are possess a high power factor. The figure of merit ZT is parameter of the performance of the thermoelectric in materials, their relation is given by the formula: $\kappa ZT = \frac{\sigma S^2 T}{}$.

A better thermoelectric performance was given by a high value of ZT, three variables are responsible for the thermoelectric performance the high density of states au round the Fermi level, the flat-dispersive band structures and the high valence band degeneracy.

We perform calculations of thermoelectric properties using the Boltztrap code [22] within relaxation time approximation, a constant relaxation time approximation, with universal $t = 10^{-14}$ s independent of the compound, was used for all calculations. This approximation is based on an assumption that relaxation time that determines electrical conductivity is not very strong at the energy scale of $k_B T$ [23].

An ample mesh of $41 \times 41 \times 41$ is used for Brillouin zone (BZ) integration. The relation of power factor ($PF = \sigma S^2$) and figure of merit contains a dynamic parameter, its The Seebeck coefficient so it's useful to see the influence of this parameter.

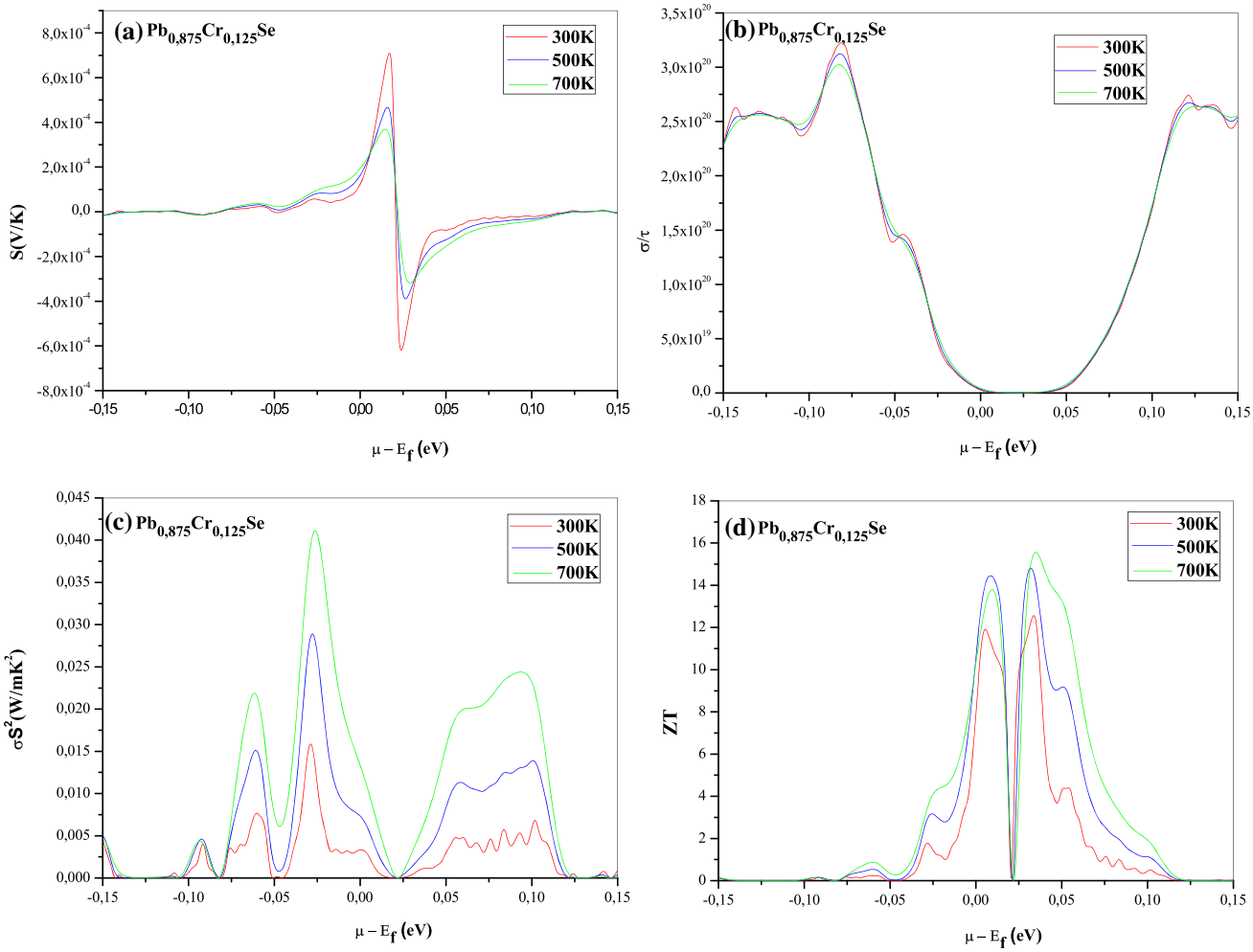

Fig. 7 Dependence of **a** Seebeck coefficients, **b** the electrical conductivity, **c** the power factor and **d** the electronic figure of merit as a function of chemical potential for three temperature of $Pb_{0.875}\,Cr_{0.125}Se$

To maximize the efficiency of thermoelectric generators, it is necessary to achieve a good thermoelectric material. Three parameter influences the importance of thermoelectric materials. First, high electrical conductivity causes charge carriers to diffuse from the hot side to the cold side and this contributes to the creation of a thermoelectric field, second a low thermal conductivity and a high Seebeck coefficient.

The Figs. 7 and 8 represents the variation of S as a function of $(\mu - E_f)$ for three temperatures. it is clear that Figs. 7a and 8a presents two peaks, which are located at energies 0.017 and 0.025 eV (0.022 and 0.028 eV) for the concentration 0.125 and 0.25 respectively. Past this interval the S tends rapidly towards zero.

At the same time, it is observed that the increase in temperature causes a decrease in S due to the increase in thermal energy. This indicates that this material has good thermoelectric performance. The negative and positive S peaks for $Pb_{0.875}\,Cr_{0.125}Se$ ($Pb_{0.75}Cr_{0.25}Se$) are -609 and 725 $\mu V\ K^{-1}$ (-479 and 583 $\mu V\ K^{-1}$) at 300 K, respectively. The total S stays positive which indicate that the holes as the majority carriers, this recommends that this is p-type material.

The effect of the electrical conductivity (σ/τ) as a function of $(\mu - E_f)$ and the variation of the temperature is projected on Figs. 7 and 8. According to Fig. 7b, the electrical conductivity reaches a minimum value in the chemical potential range [0.017, -0.022 eV] for the three temperatures 300, 500 and 700 K.

At the chemical potential -0.081 eV (-0.066 eV) at $T = 300$ K for 0.125 (0.25) concentration (see Figs. 7b, 8b), the electrical conductivity is maximum due to the increase in the concentration of carriers which causes an increase in mobility and consequently increases the conductivity.

Figures 7c and 8c shows the power factor PF Dependence of the chemical potential for three temperatures of $Pb_{0.875}Cr_{0.125}Se$ ($Pb_{0.75}Cr_{0.25}Se$). According to Fig. 7c (Fig. 8c), as the temperature increases, power factor also increases. The maximum value of power factor is located in the energy area [-0.046, 0.02 eV]. At room temperature, we found a value of the power factor equal 158.5 μ V K^{-1}. The materials-based alloys of Lead and

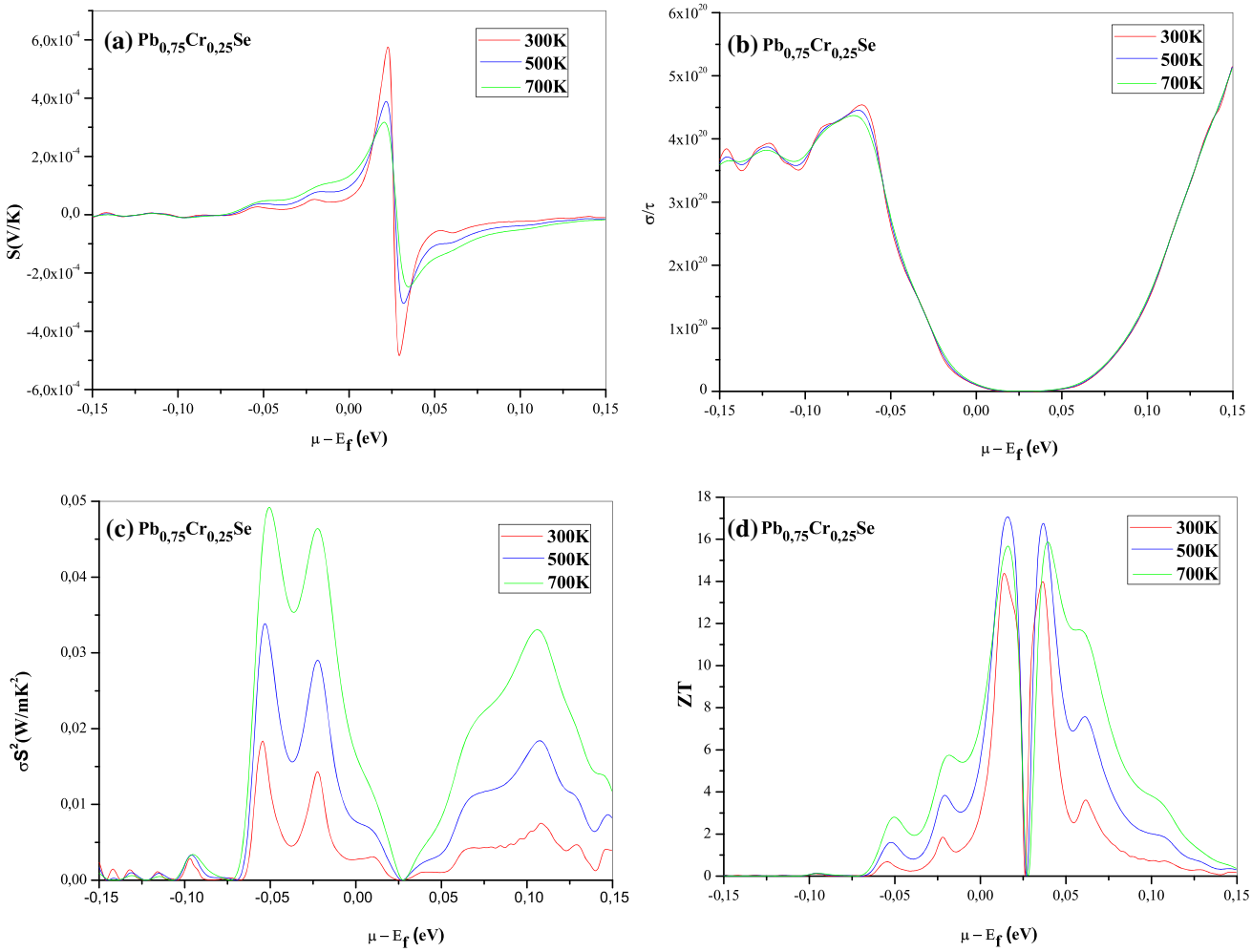

Fig. 8 Dependence of **a** Seebeck coefficients, **b** the electrical conductivity, **c** the power factor and **d** the electronic figure of merit as a function of chemical potential for three temperature of $Pb_{0.75}\,Cr_{0.25}Se$

Table 5 Calculated the electrical conductivity (σ/τ), The Seebeck coefficient, the power factor and the figure of merit at 300 K for $Pb_{1-x}Cr_xSe$ ($x = 0.125$ and 0.25)

$Pb_{1-x}Cr_xSe$	σ (10^4 Sm^{-1})	S ($\mu V\ K^{-1}$)	PF (10^{-3} W m^{-1} K^{-2})	ZT
$x = 0.125$	2.263	149.65	3.32 dn (1.36 up)	8.26 dn (0.083 up)
	4.03 [24]	−154 [23]	3.04 [23]	0.42 [23]
$x = 0.25$	7.87	668.6	2.74 dn (0.34 up)	3.06 dn (0.018 up)

in combinations Selenium are promoters for the commercial applications such as thermoelectric generators (TEGs). Next, we figure out the variation of the figure of merit as a function of chemical potential with different temperatures

For 0.125 and 0.25 concentration displayed in Fig. 7d (Fig. 8d). We see two main figures of merit ZT peaks increasing with temperature and decreasing slightly with Cr doping and then moving towards the high doping zone.

We have summarized in Table 5, the different thermal properties at room temperature for the two concentrations with comparison to the results found in literature.

The calculated the electrical conductivity, the Seebeck coefficient, the power factor and the figure of merit Z_t values for the 0.125 concentration is in reasonably good agreement with reported result in reference [24], let us quote here that the treated concentration of reference [25] is very low (0.5%).

The improvement in thermal properties such that ZT does not go through increasing the concentration of

Cr because we have lost the performance of material through the decrease in ZT.

6 Conclusion

In this manuscript, we have explored the electronic structure, magnetic and the thermoelectric properties of a $Pb_{1-x}Cr_xSe$ semiconductor with $x = 0.125$ and 0.25 from a DFT approach and Boltzmann transport theory calculations. Our analysis of Cr as dopant studied confirmed the half-metallic characteristic for our compounds with 100% spin polarization at E_F. We found a the direct band gap at Γ point in minority channel equal 0.39, 0.304 eV for $Pb_{1-x}Cr_xSe$ ($x = 0.125$ and 0.25), respectively which provoke the moving of Cr-dt_{2g} states away from EF in down spin channels for both concentration. The total magnetic moments are integral Bohr magneton with values 4 μ_B, the exchange constants proven the ferromagnetic ground state stability in these compounds. Our results give a very high seebeck value which directly influences on the power factor and therefore ZT which give an importance of these alloys for these application industrial in the thermoelectric field. to keep a high performance, we had to do with a small fraction of Cr. From the results obtained in this paper, we recommend this material studied for spintronic, optoelectronic, thermoelectronic devices.

Data Availability Statement This manuscript has no associated data or the data will not be deposited. [Authors' comment: Data is available upon request from the Authors.]

References

1. H. Ohno et al., Nature **408**, 944–946 (2000)
2. A.H. MacDonald, P. Schiffer, N. Samarth, Nat. Mater. **4**, 195–202 (2005)
3. Y. Matsumoto et al., Science **291**, 854–856 (2001)
4. T. Dietl, Nat. Mater. **9**, 965–974 (2010)
5. Q. Zhang, E.K. Chere, K. McEnaney, Adv. Energy Mater. **140**, 2015 (1977)
6. Y. Lu, S. Dong, B. Zhou, Mater. Sci. Eng. B **228**, 1–6 (2018)
7. Wang et al., J. Phys. Chem. C **123**, 30640 (2019)
8. P. Blaha, K. Schwarz, G.K.H. Madsen, D. Kvanicka, J. Luitz, *WIEN2K, An Augmented Plane Wave Plus Local Orbital Program for Calculating Crystal Properties* (Vienna University of Technology, Vienna, 2002).
9. J.P. Perdew, K. Burke, M. Ernzerhof, Phys. Rev. Lett. **77**, 3865 (1996)
10. S.B. Zhang, J.E. Northrup, Phys. Rev. Lett. **67**, 2339 (1991)
11. F.D. Muranghan, Proc. Natl. Acad. Sci. USA **30**, 244–247 (1944)
12. A. Mauger, C. Godart, Solid State Commun. **35**(10), 785–788 (1980). https://doi.org/10.1016/0038-1098(80)91074-1
13. P. Sinjukow, W. Nolting, arXiv:cond-mat/0309369 (2003)
14. M. Shafer, J. Torrance, T. Penney, J. Phys. Chem. Solids **33**(12), 2251-IN2251 (1972)
15. P. Koidl, Phys. Rev. B **15**(5), 2493 (1977)
16. X. Wang et al., Phys. Rep. **888**(13), 1–57 (2020)
17. K. Capelle, G. Vignal, C.A. Ullrich, J. Phys. Rev. B **81**, 125114 (2010)
18. A. Aharoni, *Introduction to the Theory of Ferromagnetism*, 2nd edn. (Oxford Science Publications, Oxford, 2000).
19. B.E. Larson, K.C. Hass, H. Ehrenreich, A.E. Carlsson, Phys. Rev. B **37**, 4137 (1988)
20. S. Sanvito, P. Ordejon, N.A. Hill, Phys. Rev. B **63**, 165206 (2001)
21. H. Raebiger, A. Ayuela, R.M. Nieminen, J. Phys. Condens. Matter **16**, L457 (2004)
22. G.K. Madsen, D.J. Singh, Comput. Phys. Commun. **175**, 67–71 (2006)
23. D.J. Singh, Phys. Rev. B Condens. Matter Mater. Phys. **81**, 1–6 (2010)
24. X. Wang et al., Mater. Today Phys. **6**, 45e52 (2018)
25. H. Peng, J.-H. Song, M.G. Kanatzidis, A.J. Freeman, Phys. Rev. B **84**, 3650e3754 (2011)